

Numerical study of the ordering of the $\pm J$ XY spin-glass ladder

Tsukasa Uda¹, Hajime Yoshino^{1,2} and Hikaru Kawamura¹

¹*Department of Earth and Space Science,
Faculty of Science, Osaka University,
Toyonaka 560-0043, Japan*

²*Laboratoire de Physique Théorique et Hautes Énergies, Jussieu,
5ème étage, Tour 25, 4 Place Jussieu,
75252 Paris Cedex 05, France*

(Dated: November 19, 2018)

The properties of the domain-wall energy and of the correlation length are studied numerically for the one-dimensional $\pm J$ XY spin glass on the two-leg ladder lattice, focusing on both the spin and the chirality degrees of freedom. Analytic results obtained by Ney-Nifle *et al* for the same model were confirmed for asymptotically large lattices, while the approach to the asymptotic limit is slow and sometimes even non-monotonic. Attention is called to the occurrence of the $SO(2)$ - Z_2 decoupling and its masking in spin correlations, the latter reflecting the inequality between the $SO(2)$ and Z_2 exponents. Discussion is given concerning the behaviors of the higher-dimensional models.

§1 Introduction

The domain-wall method, or the stiffness method, is widely used in studying the ordering properties of various spin systems including the spin glass (SG). In this method, one computes by some numerical means the change of the ground-state energy of finite systems of the linear dimension L under the appropriate change of boundary conditions (BCs) imposed on the system [1, 2, 3]. This energy is called a stiffness energy (or a domain-wall energy), $\Delta E(L)$, which gives a measure of an energy scale of low-energy excitations of size L . For large L , $\Delta E(L)$ is expected to behave as a power-law, $\Delta E(L) \approx L^\theta$, θ being a stiffness exponent. If $\theta < 0$, the system remains in the disordered state at any nonzero temperature, whereas if $\theta > 0$ the system possesses a finite long-range order at low enough temperatures with $T_c > 0$.

For complex systems like SGs in which the nature of the ordering is highly nontrivial, some fundamental questions still remain in this method. First question concerns with the choice of the set of BCs. In principle, there could be various choices of the set of BCs, and the behavior of $\Delta E(L)$ may depend on these choices, particularly for small sizes practically accessible in numerical simulations. It is not generally clear which set of BCs should be best chosen, especially when the results depend on the BCs. Second question concerns with the meaning of the stiffness exponent. When the domain-wall energy decreases with L , *i.e.*, the stiffness exponent is negative, it is a common practice to relate the inverse of the stiffness exponent with the correlation-length exponent ν associated with the $T = 0$ transition, *i.e.*, $\nu = 1/|\theta| = 1/y$ ($y = |\theta|$) [2, 3, 4]. By contrast, there were reports which cast doubt on the validity of this simple relation [5]. Furthermore, if the model could exhibit more than one stiffness exponents depending on the choice of the set of BCs,

a question immediately arises which stiffness exponent should be chosen to estimate the correlation-length exponent. Since, in the standard continuous (second-order) phase transition, only one diverging length scale is expected, the existence of more than one stiffness exponent poses some problem in its interpretation.

In fact, under certain circumstances, there could be more than one distinct diverging length scales, or more than one distinct correlation-length exponents, at a single continuous transition. An example of this may be seen in *chiral transitions* possibly realized in certain frustrated vector spin systems including the XY SG [6]. Frustrated vector spin systems often possesses a chirality degree of freedom due to the canted spin structure, according as the noncollinear (or noncoplanar) structure induced spin frustration is either right- or left-handed. Chirality is a pseudo-scalar variable, being invariant under global spin rotations [$SO(2)$] but changing sign under global spin reflections [Z_2]. Recent studies have suggested that some of such chiral spin systems might possibly exhibit a “spin-chirality decoupling” phenomenon, where the Z_2 chirality exhibits an ordering behavior entirely different from the $SO(2)$ spin [6], though there still remains some controversy concerning whether such a spin-chirality decoupling really occurs [6, 7, 8, 9].

In one possible realization of the spin-chirality decoupling, the chirality and the spin exhibit two separate transitions at mutually distinct temperatures, whereas, in other possible realization, the chirality and the spin order at the same temperature but with the mutually different spin and chirality correlation-length exponents, ν_s and ν_κ . Examples of the first class might be the orderings of the regularly-frustrated two-dimensional (2D) XY model [6] and those of the three-dimensional (3D) XY SG [10, 11, 12]. Examples of the second class the ordering of the regularly frustrated one-dimensional (1D) XY model [13] and those of the 2D XY SG [10, 14]. A

firmly established example is the case of the regularly-frustrated 1D XY model, where it has been shown rigorously that the spin and the chirality order at $T = 0$ where the chiral correlation length diverges exponentially with $\nu_\kappa = \infty$ but the spin correlation length as a power-law with $\nu_s = 1$ [13].

More controversial is the nature of the ordering of the XY SG. Some time ago, Kawamura and Tanemura made a numerical domain-wall study of the XY SG in 2D and 3D [10, 11]. These authors introduced various types of BCs to probe the spin and the chirality orderings of the model, including the periodic (P), antiperiodic (AP) and reflecting (R) BCs. In particular, the domain-wall energy obtained under the combination of the P and AP BCs (P/AP), $\Delta E_{P,AP}(L)$, and the one obtained under the combination of the R and P BCs, $\Delta E_c(L)$, apparently yielded mutually different stiffness exponents, which were interpreted as associated with the spin and the chiral correlation-length exponents, respectively. These authors observed that, in 2D, both $\Delta E_{P,AP}(L)$ and $\Delta E_c(L)$ decreased with L , characterized, respectively, by mutually different stiffness exponents, $y_\kappa \simeq 0.5$ and $y_s \simeq 1.0$. This observation was interpreted as indicating that the chiral correlation length outgrows the spin correlation length at the $T = 0$ transition of the model, *i.e.*, $\nu_\kappa > \nu_s$ [10]. These results were corroborated by several Monte Carlo (MC) simulations on the 2D XY SG [14, 15, 16, 17, 18, 19]. By contrast, on the basis of their domain-wall energy calculation, Kosterlitz and Akino claimed that the spin and the chiral correlation-length exponents were common at the $T = 0$ transition [7].

In 3D, Kawamura and Tanemura observed that $\Delta E_{P,AP}(L)$ ($\Delta E_c(L)$) decreased (increased) with L , which was interpreted as indicating that the chiral-glass transition occurred at a nonzero temperature, $T_{CG} > 0$, while the standard SG transition occurred only at $T_{SG} = 0$ [10, 11]. MC results supporting such a view were also reported [11, 12]. Meanwhile, later domain-wall energy calculation by Macourt and Grepel suggested that $\Delta E_{P,AP}(L)$ might eventually be iterated toward strong coupling for larger L and that $T_{CG} > T_{SG} > 0$ [20]. By contrast, Lee and Young claimed on the basis of their MC simulations that the spin and the chirality ordered at the same finite temperature $T_{CG} = T_{SG} > 0$, with a common correlation-length exponent [9] $\nu_s = \nu_\kappa$. Thus, the situation remains quite controversial.

Inspired by the numerical work of Ref.[10] on the 2D and 3D XY SG, Ney-Nifle, Hilhorst and Moore performed an analytic study of the 1D XY SG ladder with the bond-random $\pm J$ (or binary) interaction [21]. The Villain's action was assumed there. Via the dual transformation, the model was mapped onto the 1D charge Hamiltonian. Since the mapped model was still not amenable to the exact treatment, Ney-Nifle *et al* made further simplifications, and eventually derived several analytic results con-

cerning the domain-wall energies and correlation lengths. They observed that, depending on the type of the applied BCs and on whether the total number of frustrated plaquettes is either even or odd, the domain-wall energy exhibits different behaviors. When the sample average is taken over all samples, $\Delta E_{P,AP}$ is characterized by the chiral stiffness exponent $y_\kappa = 1.899 \dots$, while ΔE_c is characterized by the spin-wave (SW) stiffness exponent $y'_s = 1$. This is in contrast to the assignment made in Ref.[10] for the 2D and 3D XY SGs.

If one looks at the spin and chiral correlations of this 1D ladder model, one sees that the model exhibits the spin-chirality decoupling in the sense that there exist two distinct diverging lengths at the $T = 0$ transition (though Ney-Nifle *et al* apparently stated otherwise), the one associated with the Z_2 chirality and the other associated with the $SO(2)$ SW. The chiral correlation length ξ_κ is characterized by the exponent $\nu_\kappa = 1/y_\kappa = 0.5263 \dots$, while the SW correlation length ξ'_s is characterized by the SW exponent $\nu'_s = 1/y'_s = 1$. The full spin correlation function is the product of the Z_2 part with the correlation length $\xi_\kappa \approx T^{-0.526}$ and the $SO(2)$ part with the correlation length $\xi'_s \approx T^{-1}$. Reflecting the fact that the Z_2 chiral correlation-length exponent happens to be smaller than the $SO(2)$ SW correlation-length exponent, *i.e.*, $\nu'_s > \nu_\kappa$, the full spin correlation function is dominated by the chiral exponent ν_κ .

The analytic result of Ref.[21], though quite plausible, is not completely rigorous. Furthermore, some of the results were obtained for asymptotically large lattice. In the SG problem, it is sometimes important, and often not a trivial matter, to elucidate the finite-size effect, *e.g.*, how large the system must be for exhibiting the asymptotic large-lattice behavior.

Thus, we feel it would be useful to perform numerical study of the $\pm J$ 1D XY SG ladder in comparison with the analytic work of Ref.[21]. In the present paper, we undertake such numerical analysis of the $\pm J$ XY SG model on two-leg ladder lattices. The aim of our calculation is threefold. (i) We wish to test the validity of the simplifications made in the analytic work of Ref.[21]. (ii) We wish to elucidate the nature of the finite-size effect in this 1D model. (iii) We wish to further examine the relation between the stiffness exponents and the correlation-length exponents in this 1D model.

The following part of the paper is organized as follows. In §2, we introduce the model and summarize the analytic results of Ref.[21]. In §3, we present our numerical results of the domain-wall energies. The results are compared with those of the analytic work of Ref.[21]. Finite-size effects are analyzed carefully. In §4, we present our numerical results of the spin and chiral correlation lengths, in comparison with the corresponding analytic results of Ref.[21]. Relation with the stiffness exponents and the correlation-length exponents are examined. Finally, §5 is devoted summary and discussion.

§2. The model and some analytic formula

The model we consider is, firstly, the standard XY-SG model on the 1D two-leg ladder lattice with the binary (or $\pm J$) interaction, whose Hamiltonian is given by

$$\mathcal{H} = - \sum_{\langle ij \rangle} J_{ij} \vec{S}_i \cdot \vec{S}_j = - \sum_{\langle ij \rangle} J_{ij} \cos(\theta_i - \theta_j), \quad (1)$$

where $\vec{S}_i = (S_i^x, S_i^y) = (\cos \theta_i, \sin \theta_i)$ ($0 \leq \theta_i < 2\pi$) is the two-component spin variable at the site i , and the summation is taken over all nearest-neighbor pairs on the ladder lattice. The site index i may be written as $i = (x, y)$ with $1 \leq x \leq L$ and $1 \leq y \leq 2$, where $y = 1$ and 2 refer to the first and the second row of the ladder. J_{ij} represents the random variable taking either $+1$ or -1 with equal probability independently at each bond. The absolute value of the exchange interaction has been taken to be a unit of energy ($J = 1$).

In the following, we impose several types of BCs on the XY-spin variables at the boundary, *i.e.*, the periodic (P), antiperiodic (AP) and reflecting (R) BCs. In these P, AP and R BCs, we impose the relations, $\vec{S}_{(L+1,y)} = \vec{S}_{(1,y)}$, $\vec{S}_{(L+1,y)} = -\vec{S}_{(1,y)}$ and $\vec{S}_{(L+1,y)} = (S_{(1,y)}^x, -S_{(1,y)}^y)$, respectively. In the R BC, we reflect the spin at the boundary with respect to the x -axis in spin space.

The local chirality variable at the plaquette x , consisting of four spins at the sites $(x, 1), (x + 1, 1), (x + 1, 2)$ and $(x, 2)$, are defined by

$$\kappa_x = \frac{1}{2\sqrt{2}} \sum_{\langle ij \rangle} \text{sgn}(J_{ij}) \sin(\theta_i - \theta_j), \quad (2)$$

where the summation is taken over four bonds connecting the above four sites forming the plaquette. In the ground state of an isolated frustrated plaquette, it takes a value either $+1$ or -1 , while in the ground state of an isolated unfrustrated plaquette, it takes a value equal to zero. Thus, the states with $\kappa = \pm 1$ represent the two chiral states, with right-handed and left-handed spin circulation around the plaquette.

Other model we consider is the effective charge Hamiltonian on the dual lattice. The simplest version is the so-called Villain's Hamiltonian, which contains only the 2-body charge interaction. Although it has commonly been believed that the Villain's Hamiltonian becomes equivalent to the cosine Hamiltonian in the low-temperature limit $T \rightarrow 0$ [21], we have found that this is actually not the case: The original XY Hamiltonian mapped to the charge representation contains the higher-body interactions, in addition to the 2-body interaction, even in the $T \rightarrow 0$ limit. Thus, in the present work, we also consider these higher-body correction terms to the standard Villain's 2-body approximation [26]. The explicit forms are given in the appendix.

In the cases of the P and AP BCs, the two-body charge Hamiltonian, or the Villain's Hamiltonian, takes

the form,

$$\mathcal{H}_P = \sum_{i,j} U_{ij} m_i m_j + \frac{\pi^2}{L} (2n - \sum_i m_i - \mathcal{P})^2, \quad (3)$$

$$\mathcal{H}_{AP} = \sum_{i,j} U_{ij} m_i m_j + \frac{\pi^2}{L} (2n - \sum_i m_i - \mathcal{P} + 1)^2, \quad (4)$$

respectively, where the charge variable m_i , sitting at the plaquette i , takes integer values $0, \pm 1, \pm 2, \dots$ on unfrustrated plaquettes, and half-integer values $\pm \frac{1}{2}, \pm \frac{3}{2}, \dots$ on frustrated plaquettes. The variable n takes integer values $0, \pm 1, \pm 2, \dots$, while \mathcal{P} is the "parity" variable being equal to zero or unity depending on whether the total number of antiferromagnetic bonds on the first row ($y = 1$) of the ladder is either even or odd. The interaction between the charge variables U_{ij} located at the plaquettes i and j is defined by

$$U_{ij} = \frac{\pi^2}{L} \sum_k \frac{e^{ik(i-j)}}{2 - \cos k}. \quad (5)$$

where the summation over the wavevector k is taken over $k = 0, \pm \frac{2\pi}{L}, \pm \frac{4\pi}{L}, \dots$. In the $L \rightarrow \infty$ limit, U_{ij} reduces to

$$U_{ij} = \frac{\pi^2}{\sqrt{3}} (2 - \sqrt{3})^{|i-j|}, \quad (6)$$

which decays exponentially with distance $|i - j|$. The first term of Eq.(2) and (4) represents the charge-charge interaction, while the second term of Eq.(3) and (4) represents the SW term, which is related to the charge part via the total charge $\sum_i m_i$.

In the case of the R BC, by contrast, the corresponding two-body charge Hamiltonian is given by

$$\mathcal{H}_R = \sum_{ij} U_{ij} m_i m_j, \quad (7)$$

where U_{ij} is still given by Eq.(5), but the summation over the wavevector k is now taken over $k = \pm \frac{\pi}{L}, \pm \frac{3\pi}{L}, \dots$ which yields $U_{i+L,j} = -U_{i,j}$. Note that there is no second term (SW term) in \mathcal{H}_R .

To proceed further, Ney-Nifle *et al* made the following two assumptions [21]. First, the charge variable m_i is restricted to $\pm \frac{1}{2}$ on frustrated plaquettes and 0 on unfrustrated plaquettes. If one labels the frustrated plaquettes as $I = 1, 2, \dots, N_{\text{fr}}$, where N_{fr} is the total number of frustrated plaquettes, the chiral part of the Hamiltonian reduces to the 1D Ising Hamiltonian with N_{fr} Ising variables $\sigma_I = \pm 1$. Second, Ney-Nifle made a further simplification that the charge-charge interaction, which originally work between arbitrary pairs of frustrated plaquettes, is restricted only to the nearest-neighbor pairs of frustrated plaquettes. After these two simplifications,

the model reduces to the 1D Ising chain with the random antiferromagnetic nearest-neighbor interaction,

$$\mathcal{H}_{\text{Ising}} = \sum_{I=1}^{N_{\text{fr}}} V_I \sigma_I \sigma_{I+1}. \quad (8)$$

The random nearest-neighbor interaction $V_I > 0$ obeys the distribution given by

$$P(V) = cV^{-1+\nu_\kappa}, \quad \nu_\kappa = 0.5263 \dots, \quad (9)$$

for smaller V , where c is a normalization constant. The latter simply follows from Eq.(6) and the fact that the probability to have a sequence of l successive unfrustrated plaquettes is given by $1/2^l$. Thus, it should be remarked that the distribution of the effective interactions $P(V)$ is not a smooth function but a collection of delta functions so that Eq.(9) must be taken with care.

These simplifications enabled Ney-Nifle *et al* to specify the explicit charge (chirality) pattern and the existence/non-existence of the SW excitation in the ground state of large enough lattices under the given BC, leading to various predictions on the domain-wall energies and the correlation lengths.

§3. Numerical results on the domain-wall energies

In this section, we numerically calculate the following two types of domain-wall energies for the 1D XY SG ladder, *i.e.*, (i) the root-mean square of the energy difference between under the P and AP BCs, $\Delta E_{\text{P,AP}}$, and (ii) the absolute value of the energy difference between under the R and min(P,AP) BCs, ΔE_c , where min(P,AP) refers to either P or AP BC which has the lower energy than the other. The following three levels of numerical calculations are made.

Method (A): The first method is the direct numerical estimate of the ground-state energy of the cosine Hamiltonian of finite L under the given BC. In calculating the ground-state energy, we employ the spin-quench algorithm without any further approximation, *i.e.*, by starting from the randomly generated spin initial conditions, we quench the system to reach one of the local energy minima. These quench procedures are repeated many times, typically 5,000 times, until one is sure that the true ground state has been reached. If one goes to larger L , the number of local minima increases rapidly which makes the search of the true ground state increasing difficult. This difficulty limits the tractable maximum lattice size to $L \leq 35$. The sample average is taken over 10,000 ($L = 35$) - 200,000 ($L \leq 15$) independent bond realizations.

Methods (B1)-(B3): In this group of methods, we estimate the ground-state energy of the effective charge Hamiltonian of finite L under the given BC within the first approximation of Ref.[21]. Namely, we use the Ising

Hamiltonian but with the distant-neighbor interaction in estimating the domain-wall energy. In identifying the chirality pattern of the ground state (or the candidate of the ground state), we have made certain plausible assumptions, the detail of which will be given below for each different case: It is similar to the procedure employed in Ref.[21], but it is systematically improved in the estimation of the domain wall energies by taking into account the distant-neighbour two-body interactions and also the higher-body interactions. By the methods (B1)-(B3), we examined lattices considerably larger than the case (A), up to $L = 960$. The sample average is taken over 100,000 independent bond realizations.

Method (C): In this third method, we estimate the ground-state energy of the Villain's Hamiltonian of finite L under the given BC by assuming both the first and the second approximations of Ref.[21]. Namely, we use the Ising Hamiltonian with the nearest-neighbor interaction in estimating the domain-wall energy. In this case, we can deal with lattices still larger than the cases (B1)-(B3), and the results for asymptotically large L should reduce to the analytic results of Ref.[21]. The sample average is taken over 100,000 independent bond realizations.

We compare the results of these five levels of calculations (A), (B1)-(B3) and (C) to examine the validity of the approximations made in Ref.[21], and to elucidate the nature of the finite-size effects in this model.

In the original cosine model (1), the local chirality at each plaquette is given by Eq.(2). In the ground-state, the *local* chirality distribution is expected to be peaked around $\kappa = \pm 1$ for frustrated plaquettes, and around $\kappa = 0$ for unfrustrated plaquettes. We have checked numerically that this is indeed the case. As shown in Fig.1, the local chirality on frustrated plaquettes takes the values around $\kappa \simeq \pm 1$ with equal probability, while that on unfrustrated plaquettes takes the values around $\kappa = 0$. Such a distribution of the local chirality enables us to label the chirality pattern uniquely only by the combination of + and - on frustrated plaquettes.

In the present 1D model, as was first suggested by Ney-Nifle *et al* [21], the behavior of the domain-wall energy largely depends on whether the total number of frustrated plaquettes N_{fr} is either even or odd. We call these samples "even" and "odd" samples, respectively. In what follows, we show the results for the even and odd cases separately.

§3.1 Even samples

3.1.1 The domain-wall energy: $\Delta E_{\text{P,AP}}$

For even samples, Ref.[21] predicted that the domain-wall energy $\Delta E_{\text{P,AP}}$ was dominated for large enough lattices by the contribution of a pair of chiral domain-wall excitations not accompanying the SW excitation. The

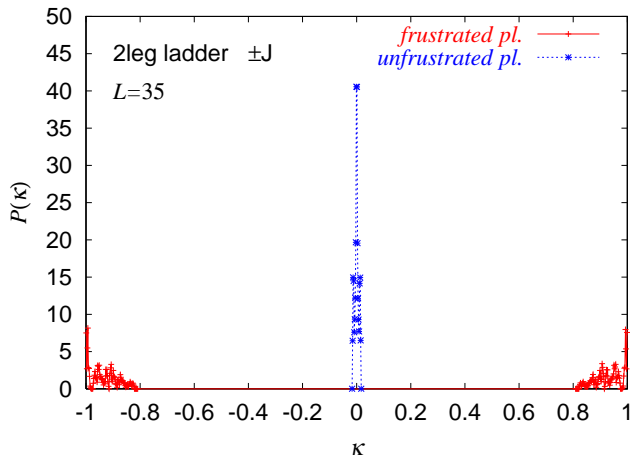


FIG. 1: The distribution function of the local chirality κ at each plaquette in the ground state of the $\pm J$ XY ladder. The lattice size is size $L = 35$. The data for frustrated and unfrustrated plaquettes are given in blue (at the center $\kappa = 0$) and in red (near the edges $\kappa = \pm 1$), respectively.

chiral domain-wall may be defined here as the “chiral overlap” between the two chirality configurations 1 and 2 under the two BCs, $O_i = m_i(1)m_i(2)$, changes the sign. According to Ref.[21], under the min(P,AP) BC, the sign of the chirality pattern alternates on frustrated plaquettes without misfit, while under the max(P,AP) BC, a pair of misfits is introduced into the alternating chirality pattern, but not accompanying the SW excitation: A pair of chirality misfits is introduced into the sample in such a way that one is at the weakest connection, *i.e.*, the place where the neighboring frustrated plaquettes are most far apart in distance, and the other is at the next-weakest connection satisfying the condition $\sum_i m_i = \pm 1$. The latter condition is required to suppress the SW term in eqs.(3) or (4). The other possible candidate of the ground state under the max(P,AP) BC might be the π -SW state with a nonzero second term but without any misfit in the alternating chirality pattern. However, if the assumptions made in Ref.[21] are to be justified, the chiral domain-wall state always has the lower energy than the SW state, at least in sufficiently large lattices.

In our methods (B1)-(B3) above, we search for the positions of a pair of chiral domain walls in the ground state under the max(P,AP) BC according to the following procedure. First, to specify the position of one of the two chiral domain walls, we apply the R BC to the same sample. The application of the R BC is expected to yield a single chiral domain wall in the sample: See below. By calculating and comparing the energies corresponding to all possible N_{fr} positions of a chiral domain wall, we determine the position of the chiral domain wall in the ground state under the R BC. This position is as-

sumed to be common with the position of one of the two chiral domain walls introduced under the max(P,AP) BC. We then determine the position of the second chiral domain wall in the ground state under the max(P,AP) BC by calculating and comparing the energies corresponding to all possible positions of the second chiral domain wall under the constraint that there are odd number of frustrated plaquettes between the two chiral domain walls. In calculating the energy, we employ systematically improved methods (B1)(B2) and (B3) unlike the case of our method (C) which takes into account the nearest-neighbour interaction only. In the method (B1), we use the two-body approximation but sum over all distant-neighbor interactions. In the methods (B2) and (B3), we take into account the higher-body correction terms up to the 4-body and 6-body interactions, respectively. The explicit forms of the higher-body terms are given in the appendix.

In our direct method (the method (A) above) for finite $L \leq 35$ samples, we have observed that, under the min(P,AP) BC, the rule of the ground-state configuration of [21] is always satisfied, while, under the max(P,AP) BC, some samples obey the rule of Ref [21], but some other samples do not. In the latter class of samples, the ground state under the max(P,AP) BC turns out to be the π -SW state rather than the chiral domain-wall state, *i.e.*, the chirality pattern completely alternate without misfit while the SW of a turn angle π (π -SW) is generated between under the P and AP BCs. An example of such a π -SW sample is shown in Fig.2, where the spin configurations under the P and AP BCs are shown in the upper panel of Fig.2, while the relative deviation angle between the spin directions under the P and AP BCs is illustrated in the lower panel by arrows. The appearance of the π -SW is clearly visible here. Hence, at least in a subset of samples of finite $L \leq 35$, the rule of Ref.[21] is violated.

The domain-wall energy $\Delta E_{\text{P,AP}}$ calculated in our direct method (A) is shown in Fig.3(a) on a log-log plot. The slope is estimated to be about 1.39 in the range $L \leq 35$, which is considerably smaller than the predicted value of Ref.[21], $1.899 \dots$, presumably due to the existence of the SW samples characterized by the SW stiffness exponent $y'_s = 1$.

Then, the next question is how the rate of the π -SW samples, which breaks the rule of Ref.[21], varies with increasing L . This rate of the SW samples r_{SW} calculated in the direct method (A) is shown in Fig.4(a) in the range $L \leq 35$. As can be seen from figure, while the rate decreases with increasing L for smaller lattices of $L \lesssim 20$, it tends to *increase again* for larger lattices up to $L = 35$. Unfortunately, the direct calculation is limited to $L = 35$.

The rate of the SW samples r_{SW} is also estimated by using the Ising approximation (the method (B1)-(B3)) and the nearest-neighbor approximation (the method

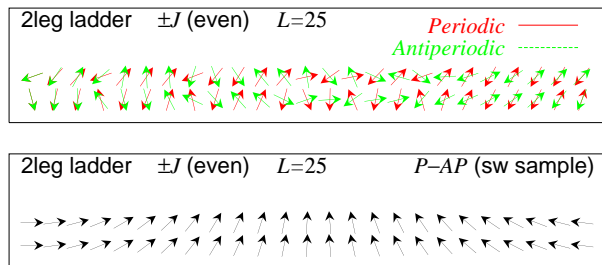


FIG. 2: A typical example of the ground-state spin configuration of even samples under the periodic and antiperiodic boundary conditions, between which a spin-wave of a turn angle π is generated. The lattice size is $L = 25$. In the lower panel, the relative deviation angle between the spin directions under the periodic and antiperiodic boundary conditions is illustrated by arrows.

(C)), and the results are also shown in Fig.4(a) in the same range of $L \leq 35$. One sees from the figure that the rate calculated by both approximations exhibits the non-monotonic behavior qualitatively similar to the one observed by the direct method (A). In particular, the Ising approximation (B1)-(B3) gives the results in quantitative agreement with those of the direct method (A). The quantitative agreement becomes systematically better by including the distant-neighbour two-body interactions (B1), 4-body interactions (B2) and 6-body interactions (B3).

By contrast, the nearest-neighbor approximation (C) yields the results which considerably deviates from the results of the direct method quantitatively, although some qualitative features are still captured.

In order to investigate the behavior of larger lattices $L \geq 35$, we have to rely on the approximate methods (B1)-(B3) and (C). The domain-wall energy $\Delta E_{P,AP}$ and the rate of the SW sample r_{SW} calculated for larger lattices $L \geq 35$ by the methods (B1)-(B3) and (C) are shown in Figs.3(b) and 4(b), respectively. In both methods, the ground state under the given BC is searched for between the chiral domain-wall state and the π -SW state by comparing the energies of these two states. As can be seen from Fig.4(b), the rate of the SW sample r_{SW} , once increased with L at $L \leq 35$, decreases with further increasing L and tends to zero in the $L \rightarrow \infty$ limit but with peculiar oscillations. Likewise, as can be seen from Fig.3(b), $\Delta E_{P,AP}$ yields a slope close to 1.9 for large enough L , consistent with the value of Ref.[21]. Thus, the asymptotic large- L behavior seems consistent with

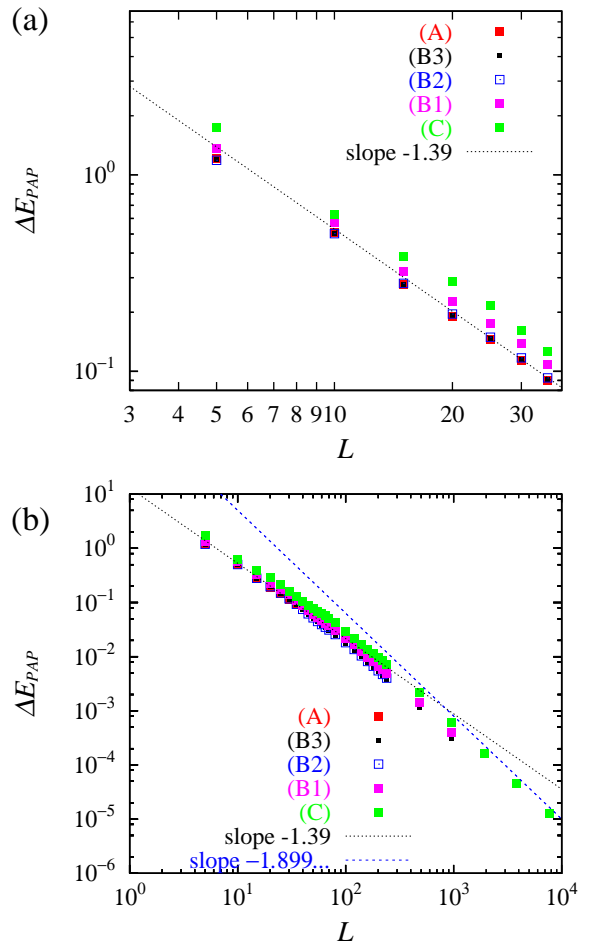


FIG. 3: The domain-wall energy $\Delta E_{P,AP}$ of even samples, calculated by the three methods (A), (B1)-(B3) and (C) mentioned in the text, are plotted versus L on a log-log plot. The dotted line is the power law $L^{-1.899\dots}$ predicted in Ref. [21].

Ref.[21], while the approach to the large- L asymptote is rather slow, realized only for lattices with $L \gtrsim 40$.

Of course, the methods (B1)-(B3) and (C) assume properties of the ground-state configurations are not completely rigorous. However, the fact that the non-trivial (non-monotonic) small- L behavior revealed by the direct method (A) is also reproduced by these approximate methods gives some credence to the reliability of the approximate methods even for larger L where the direct method is not available.

In Fig.5, we show the distribution function of the domain-wall energy $\Delta E_{P,AP}$ for the sizes of $L = 35$, Fig. 5 (a), and $L = 240 - 960$, Fig. 5 (b). As can be seen from Fig. 5(a), the SW samples contributes the component near the edge of the distribution whose weight decreases with increasing L . Interestingly, the distribution is not smooth at all. As L increases, more bands of spikes appear closer to the center $\Delta E_{P,AP} = 0$ and

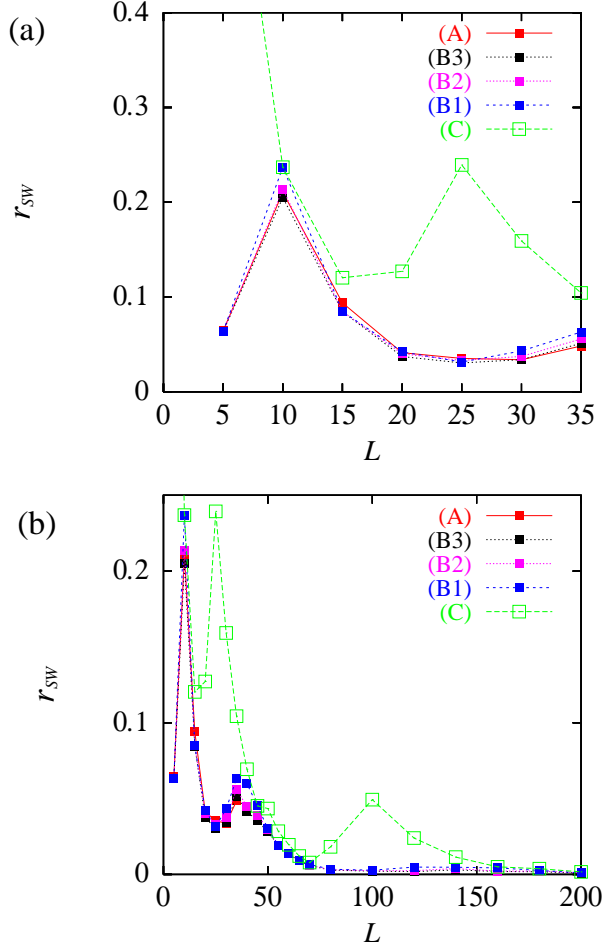


FIG. 4: The L -dependence of the rate of the spin-wave samples within the even samples under the periodic boundary condition, calculated by the three methods (A), (B1)-(B3) and (C) mentioned in the text.

the amplitude of the spikes at smaller $|\Delta E_{P,AP}|$ becomes larger. Presumably the bands of the spikes reflect nearly discrete spectrum of the distribution of effective interactions between chiralities, which is not explicit in Eq. (9).

3.1.2 The domain-wall energy: ΔE_c

Now, we turn to the second type of domain-wall energy, ΔE_c , the absolute value of the ground-state energy difference between under the R and min(P,AP) BCs. Under the R BC, the sign of the chirality is reversed at the boundary. Therefore, if the sign change in the chiral-overlap $O_i = m_i(\text{R})m_i(\text{min(P, AP)})$ occurs at the boundary, it actually means that there is no chiral domain-wall at the boundary. With this understanding, under R/min(P,AP) of even samples, a single chiral domain-wall should be introduced into the sample, not accompanying the SW excitation[21]. Hence, ΔE_c should be characterized by the chiral stiffness exponent $y_\kappa = 1.899 \dots$.

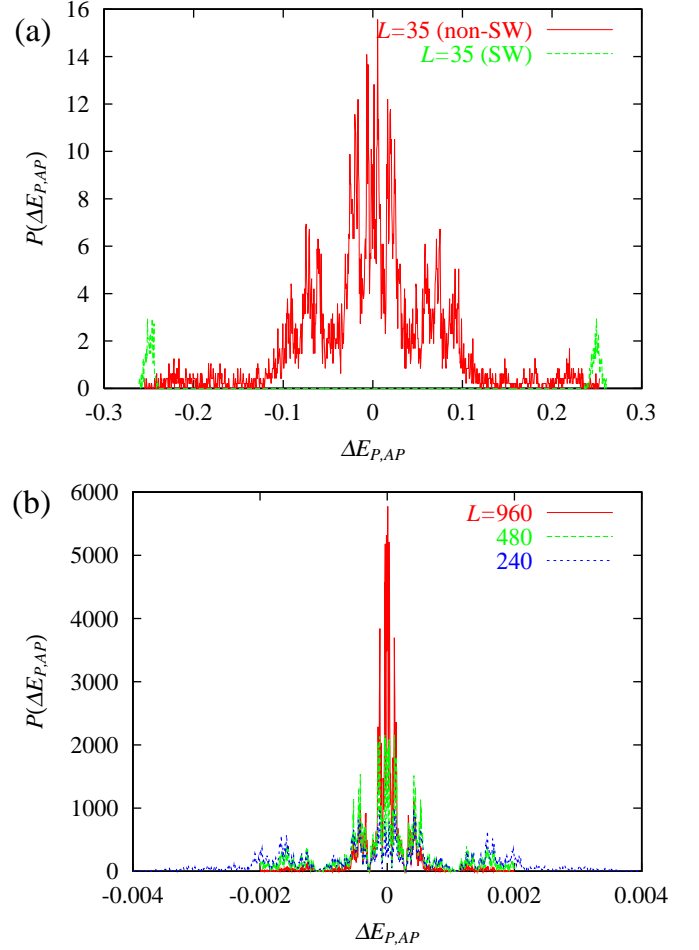


FIG. 5: The distribution function of the domain-wall energy $\Delta E_{P,AP}$ for even samples with $L = 35$ obtained by the method (A) (a), and $L = 240, 480, 960$ obtained by the method (B1) (b).

Indeed, our direct method (A) has fully confirmed this expectation.

In Fig.6(a), we show the size dependence of the domain-wall energy, ΔE_c , estimated by the three methods (A), (B1)-(B3) and (C). As mentioned in §3.1.1, in the method (B1)-(B3), the position of a chiral domain wall is determined by calculating and comparing the energies corresponding to all possible N_{fr} positions of a chiral domain wall. In the size range $L \leq 35$ where the direct calculation is available, the data yield a slope about 1.58, which is considerably smaller than the expected value $y_\kappa = 1.899 \dots$. However, the data for larger lattices obtained by the approximate methods (B1)-(B3) and (C) yield an asymptotic slope consistent with the expected value $y_\kappa = 1.899 \dots$. Again, the approach to the asymptotic behavior turns out to be rather slow.

3.2 Odd samples

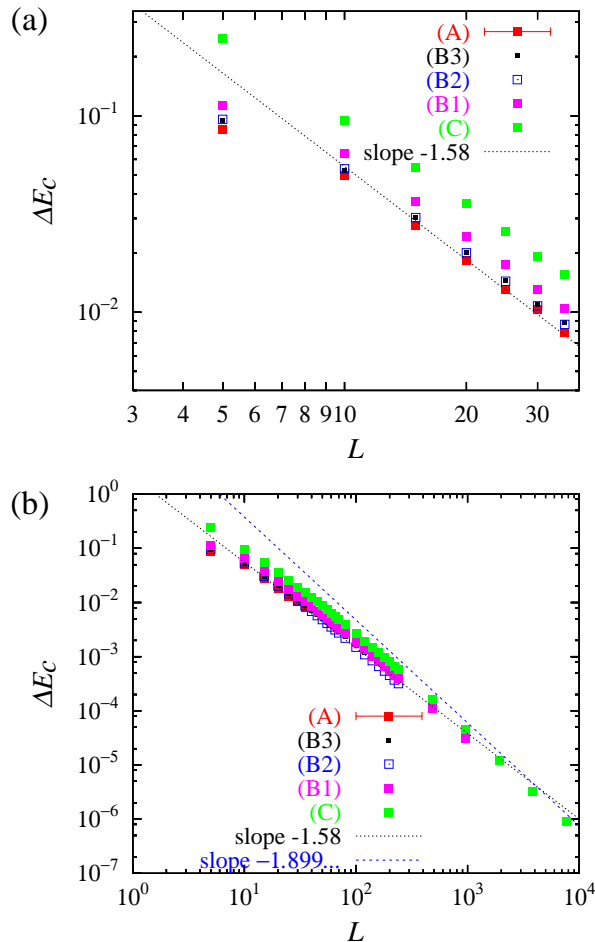


FIG. 6: The domain-wall energy ΔE_c of even samples, calculated by the three methods (A), (B1)-(B3) and (C) mentioned in the text, are plotted versus L on a log-log plot. The dotted line is the power law $L^{-1.899\dots}$ predicted in Ref. [21].

In this subsection, we deal with the other subset of samples where the total number of frustrated plaquettes is odd.

3.2.1 The domain-wall energy: $\Delta E_{P,AP}$

For odd samples, Ref.[21] shows that the P and AP BCs always yield exactly the same ground-state energy, *i.e.*, $\Delta E_{P,AP} = 0$. In the ground-state chirality pattern, a single misfit is introduced into the alternating chirality pattern, but always in the same position between under the P and AP BCs so that there is no chiral domain-wall between under the P and AP BCs. Instead, the π -SW is generated between them. Indeed, we have confirmed this expectation by the direct method (A).

3.2.2 The domain-wall energy: ΔE_c

In the case of R/min(P,AP) of odd samples, a single chiral domain-wall is expected to be introduced with accompanying the $\pi/2$ -SW[21]. This has been confirmed

by our direct method (A). A typical example of the spin configurations under the R and P BCs is shown in Fig.7. The existence of the $\pi/2$ - SW is clearly visible.

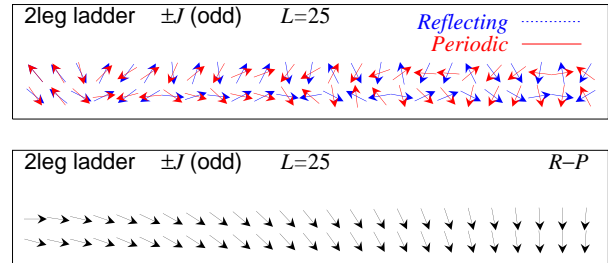


FIG. 7: A typical example of the ground-state spin configuration of odd samples under the periodic and reflecting boundary conditions, between which a spin-wave of a turn angle $\pi/2$ is generated. The lattice size is $L = 25$. In the lower panel, the relative deviation angle between the spin directions under the P and R BCs is illustrated by arrows.

Here, the domain-wall energy, ΔE_c , is expected to be a sum of the chiral domain-wall contribution characterized by the chiral exponent $y_\kappa = 1.899\dots$ and the SW contribution characterized by the SW exponent $y'_s = 1$ [21]. For large enough L , a slowly-decaying component, *i.e.*, the SW component, should dominate the asymptotic behavior of ΔE_c . In Fig.8, we show on a log-log plot the L -dependence of the domain-wall energy, ΔE_c , calculated by our methods (A), (B1)-(B3) and (C). In the methods (B1)-(B3), the position of a single chiral domain wall is determined by calculating and comparing the energies corresponding to all possible N_{fr} positions of a chiral domain wall. In the size range $L \leq 35$ where the direct calculation is available, the data yield a slope about 1.07, which is slightly larger than the expected asymptotic value $y_\kappa = 1$. This deviation for smaller L might be due to the residual contribution of the chiral domain-wall. Meanwhile, the data for larger lattices obtained by the approximate methods (B1)-(B3) and (C) yield the asymptotic slope fully consistent with the expected value, $y = 1$.

3.3 All samples

As shown above, the behaviors of the domain-wall energy largely differ between in even and odd samples. The behavior observed when one measures the domain-wall energy averaged over all samples can be obtained immediately by simply combining the above results for even and odd samples with equal weights.

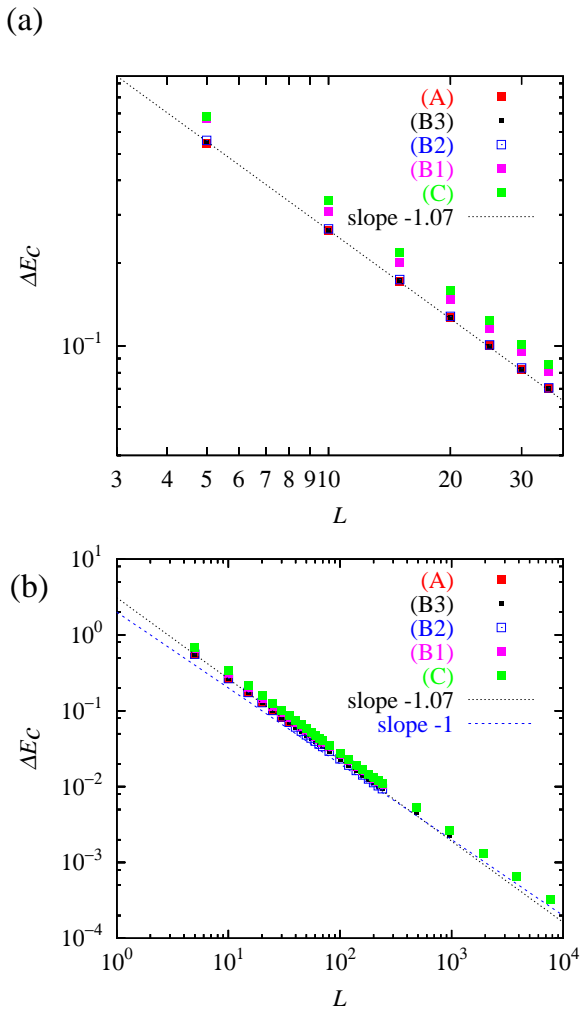


FIG. 8: The domain-wall energy ΔE_c of odd samples, calculated by the three methods (A), (B1)-(B3) and (C) mentioned in the text, are plotted versus L on a log-log plot.

The behavior of $\Delta E_{P,AP}$ averaged over all samples is exactly the same as that for even samples, since $\Delta E_{P,AP}$ is identically zero for odd samples. It exhibits an asymptotic behavior characterized by the stiffness exponent $y_\kappa = 1.899 \dots$ for large enough L , while there is a significant finite-size correction and the asymptotic behavior sets in only at $L \gtrsim 40$.

By contrast, ΔE_c is a sum of the chiral contribution and the SW contribution, the large- L behavior being dominated by the latter. Hence, ΔE_c averaged over all samples is asymptotically characterized by the SW exponent $y'_s = 1$, in contrast to $\Delta E_{P,AP}$.

These asymptotic behaviors were just as predicted by Ney-Nifle *et al* [21].

§4. Numerical results of the correlation length

In this section, we numerically investigate the temperature dependence of the spin and the chiral corre-

lation lengths, ξ_s and ξ_κ , with interest in the associated correlation-length exponents, ν_s and ν_κ . Since the correlation functions are bulk quantities, one usually believes that they are independent of the type of BCs, or whether the sample is either even or odd, in contrast to the case of the domain-wall energies analyzed in the previous section. Indeed, this was implicit in the analysis of Ref.[21].

The two-point spin-spin and chirality-chirality correlation functions, $C_s(R)$ and $C_\kappa(R)$, are defined by

$$C_s(R) = [\langle \vec{S}_{(0,1)} \cdot \vec{S}_{(R,1)} \rangle^2], \quad (10)$$

$$C_\kappa(R) = [\langle \kappa_0 \kappa_R \rangle^2], \quad (11)$$

where $\langle \dots \rangle$ denotes the thermal average and $[\dots]$ denotes the average over the bond disorder.

We directly calculate these correlation functions of the cosine model under the P BC by means of the standard Monte Carlo simulation. The spin and the chiral correlation lengths are extracted by fitting the calculated correlation functions by a simple exponential form, $A \exp[-(r/\xi)]$ (A is a constant). To guarantee that the estimated correlation lengths are free from the finite-size effect, the data are limited to the temperature region $T/J \geq 0.1$ where both correlation lengths ξ_s and ξ_κ are much smaller than the system size $L = 100$. At the temperature $T/J = 0.1$, ξ_s and ξ_κ become around 6 and 3, respectively. In order to be sure that the correlation lengths are insensitive to whether the sample is even or odd, we estimate ξ_s and ξ_κ for each case of even and odd samples. As expected, ξ_s of even and odd samples agree within the error bars, so does ξ_κ .

In Fig.9(a), we show on a log-log plot the temperature dependence of ξ_s and ξ_κ averaged over all samples, total number of samples being 100. As can be seen from Fig.9(a), in the investigated temperature range $T/J \geq 0.1$, the data yield a slope close to unity for both ξ_s and ξ_κ . This value, unity, may be related to the SW stiffness exponent $y'_s = 1$ via the relation $\nu = 1/y$. It is significantly smaller than the asymptotic value obtained in Ref.[21] $\nu_s = \nu_\kappa = 1/y_\kappa = 0.5263 \dots$. However, since the temperature range covered in the present simulation is rather high and the correlation lengths still stayed shorter than the crossover length ~ 40 estimated in the previous section, it is quite probable that we need to go to lower temperatures to see the true asymptotic critical behavior associated with the $T = 0$ transition. Unfortunately, we cannot directly evaluate the correlation lengths in this low temperature region because of the finite-size effect and the thermalization problem.

Ney-Nifle *et al* gave an analytic expression of the spin and the chiral correlation lengths in the thermodynamic limit on the basis of the two assumptions mentioned above [21]. The chiral correlation function is obtained as

$$C_\kappa(R) = [\langle 2m_0 \cdot 2m_R \rangle^2] \quad (12)$$

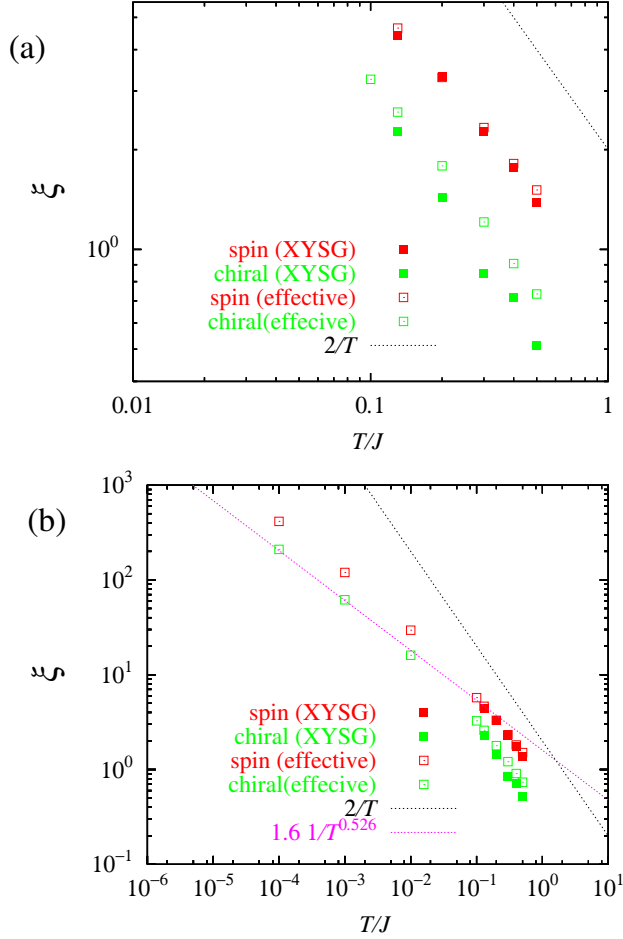


FIG. 9: The temperature dependence of the spin and the chiral correlation lengths, ξ_s and ξ_κ , of the bulk sample, estimated by Monte Carlo simulation and numerical analysis of the effective charge model.

$$= \left[\prod_{j=1}^S \tanh^2 \left(\frac{V_j}{k_B T} \right) \right] \quad (13)$$

$$= e^{-R/\xi_\kappa}, \quad (14)$$

where T is the temperature. In Eq. (13), the product is taken over all nearest-neighbor effective bonds V_j which lie in the section between the sites 0 and R and are labeled as $j = 1, 2, \dots, S$ where S is the number of frustrated plaquettes between the sites 0 and R . The chiral correlation length ξ_κ behaves in the $T \rightarrow 0$ limit as

$$\xi_\kappa \sim \frac{1}{T^{\nu_\kappa}} \quad \nu_\kappa = 1/\nu_s = 0.5263 \dots \quad (15)$$

In the Villain model, the spin correlation function is obtained as

$$C_s(R) = [\langle \cos(\theta_{(0,1)} - \theta_{(R,1)}) \rangle^2] \quad (16)$$

$$= e^{-R/\xi'_s} C_{\text{charge}}(R), \quad (17)$$

where the SW correlation length ξ'_s is given by

$$\xi'_s = \frac{2}{T}. \quad (18)$$

Here the spin correlation function is factorized into the two parts, one due to the SW and the other due to the charges C_{charge} . Within the effective model studied by Ney-Nifle *et al* [21], *i.e.* the Ising model with the nearest-neighbor random antiferromagnetic interaction, the charge part becomes,

$$C_{\text{charge}}(R) = \left[\prod_{k=1}^{S/2} \tanh^2 \left(\frac{V_{2k}}{k_B T} \right) \right] \quad (19)$$

$$= e^{-R/2\xi_\kappa}. \quad (20)$$

In the cases where S is an odd integer, the charge (chiral) correlation function vanishes. These results do not depend on the type of BCs nor on whether the sample is either even or odd.

In Fig.9, we show these analytic results of the spin and chiral correlation lengths for the effective model together with the corresponding MC estimates for the original XY SG model. In our analytic calculations, we evaluated the averages over the disorder in Eq.(13) and Eq.(19) taking into account the true discrete spectrum of the distribution of spacings between frustrated plaquettes rather than using the continuous expression Eq.(9). As can be seen from Fig 9(a), in the higher temperature range $T/J \geq 0.1$, the analytic results of Ref.[21] agree with our MC results, exhibiting the near $1/T$ -behavior. Such an agreement observed at higher temperatures might give some credence to the reliability of the approximate methods. At lower temperatures where the MC result is no longer available, the analytic results of Ref.[21] tend to level off, exhibiting a clear crossover. There, for both cases of ξ_s and ξ_κ , a power-law behavior with a much smaller asymptotic exponent $\nu_s = \nu_\kappa = 0.5263 \dots$ are eventually realized. The crossover from the $1/T$ behavior to the $1/T^{0.5263 \dots}$ behavior occurs below $T/J \simeq 0.1$, at the length scale of $L = 30$ lattice spacings. This crossover might be related to the domain-wall result in the previous section where a crossover takes place at around $L = 40$.

Hence, the asymptotic critical behavior of the spin and chiral correlation lengths sets in only at low temperatures $T/J \lesssim 0.1$ and at longer length scale $\xi \gtrsim 30$. At higher temperatures $T/J \gtrsim 0.1$ and at shorter length scale $\xi \lesssim 30$, a different power-law behavior with an apparent exponent $\nu \simeq 1$ fits the data better.

It might be worth emphasizing here again that, although the spin and the chiral correlation lengths exhibit the same critical behavior, apparently with only one diverging length scale, there in fact exist two distinct length scales at the $T = 0$ transition of this model. This has been already evident in Eqs. (17) and (20),

where the spin correlation function is written as a product of the Z_2 chiral part, characterized by the correlation length with the chiral exponent $\nu_\kappa = 0.5263 \dots$ and the $SO(2)$ SW part, characterized by the correlation length with the SW exponent $\nu'_s = 1$. Hence, while there actually exist the two diverging length scales at the $T = 0$ transition of the model, the one diverging more slowly, *i.e.*, the one with smaller ν , dominate the asymptotic behavior of spin correlations, masking the existence of the other correlation length which diverges more rapidly.

We note that such a “masking” phenomenon arises only when the inequality $\nu_\kappa < \nu'_s$ holds between the Z_2 and $SO(2)$ correlation-length exponents. If this inequality would be opposite, the masking phenomenon would not show up in the spin correlations. Then, the existence of two correlation lengths would manifest itself more directly in the associated correlation functions, the $SO(2)$ spin correlation length in the spin correlations and the Z_2 chiral correlation length in the chiral correlations. This actually occurs in the aforementioned regularly frustrated 1D XY model, where one has $\nu_\kappa = \infty > \nu'_s = 1$ as shown rigorously for the case of 1D triangular lattice in Ref. [13].

Naturally, one expects essentially the same behavior in the present two-leg ladder XY model. Let us consider the regularly frustrated two-leg ladder XY model such that all spacings between frustrated plaquettes are equal to l . The analytic expressions of the charge (chirality) and the spin correlation functions, Eqs.(13) and (19), expected to be valid at low enough temperatures $T/J \ll 1$, can also be used in the regular case where the average over the bond disorder should be dropped. As examples, we show in Fig.10 the temperature dependence of the spin and the chiral correlation lengths ξ_s and ξ_κ for the cases of $l = 2$ and 4. As can be seen from the figure, the chiral correlation length ξ_κ outgrows the spin correlation length ξ_s at some finite temperature T_\times . At higher temperatures $T > T_\times$, ξ_s and ξ_κ exhibit a more or less similar behavior with $\xi_s > \xi_\kappa$. At lower temperatures $T < T_\times$, while ξ_κ continues to exhibit a behavior similar to the behavior observed at higher temperatures $T > T_\times$, the spin correlation length ξ_s dramatically changes its behavior. The growth of ξ_s with the decrease of the temperature is dramatically slowed down below T_\times yielding $\xi_s \ll \xi_\kappa$; a manifestation of the spin-chirality decoupling.

§5. Summary and discussion

We numerically investigated the domain-wall energies and the spin and the chiral correlation lengths of the 1D $\pm J$ XY SG ladder. Analytic results obtained by Ney-Nifle *et al* were confirmed for asymptotically large L , while the finite-size effect could be significant. Concerning the domain-wall energies, the asymptotic behavior sets in only for lattices with $L \gtrsim 40$. Concerning the

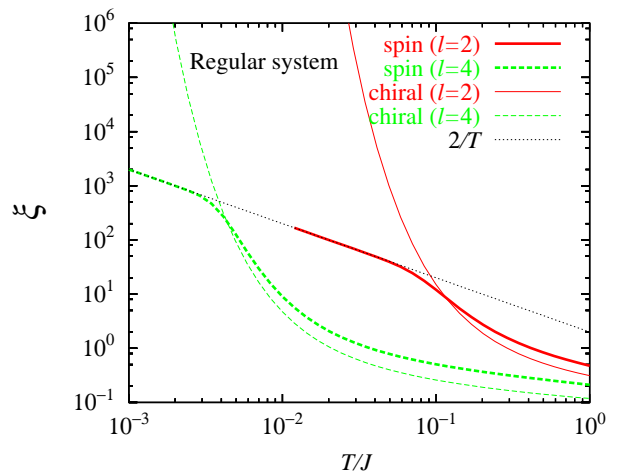


FIG. 10: The temperature dependence of the spin and the chiral correlation lengths, ξ_s and ξ_κ , of the two-leg ladder regularly frustrated XY model evaluated by the effective charge model. The spacings between frustrated plaquettes are equal to l . Here the results of $l = 2$ and $l = 4$ are shown as examples.

correlation lengths, the asymptotic behavior sets in only at low temperatures $T/J \lesssim 0.1$.

The domain-wall energies show different behaviors depending on the type of BCs and whether the number of frustrated plaquettes is even or odd. The domain-wall energy associated with the P/AP BCs, $\Delta E_{P,AP}$, is identically zero for odd samples, and exhibits a rather complex behavior for even samples. For even samples, although the lowest-energy excitation is always a chiral-domain wall pair for asymptotically large L , the one for smaller L is sometimes a π -SW without accompanying the chiral domain wall, which eventually gives way to the chiral domain-wall pair excitation for larger L . Somewhat unexpectedly, the approach to the asymptotic large- L limit is rather slow and could be even non-monotonic (see Fig.4(b)), and the asymptotic large- L behavior sets in only at $L \gtrsim 40$. The chiral domain wall and the SW bear the associated stiffness exponents, $y_\kappa = 1.899 \dots$ and $y'_s = 1$, respectively. We note that, if the inequality between y_κ and y'_s would be opposite, *i.e.*, if $y_\kappa < y'_s$, then $\Delta E_{P,AP}$ would be characterized by y_s , not by y_κ .

The domain-wall energy associated with the R/min(P,AP) BC, ΔE_c , is governed by a chiral domain-wall excitation, with and without the SW for odd and even samples. Absence or presence of the SW excitation gives rise to the different asymptotic behaviors of ΔE_c for even and odd samples, respectively. The SW excitation, whenever it is induced, governs the large- L asymptotic behavior of the domain wall energy since $y'_s = 1 < y_\kappa = 1.899 \dots$ in the present model. Thus, ΔE_c is characterized by an asymptotic stiffness exponent $y = y_\kappa$ and $y = 1$ for even and odd samples,

respectively. We emphasize again that, if the inequality between y_κ and y'_s would be opposite, ΔE_c would always be characterized by the chiral exponent y_κ for both even and odd samples.

We also numerically investigated the behavior of the spin and the chiral correlation lengths. Both exhibit the divergence characterized by the chiral exponent $\nu_\kappa = 1/y_\kappa = 0.5263 \dots$, whereas this asymptotic behavior sets in only at low temperatures $T/J \lesssim 0.1$ and at longer length scale $\xi \gtrsim 30$. At higher temperatures $T/J \gtrsim 0.1$ and at shorter length scale $\xi \lesssim 30$, a different power-law behavior characterized by an apparent exponent $\nu \simeq 1$ is realized. Although both the spin and the chiral correlation lengths exhibit the critical behavior with a common exponent y_κ , the system in fact possesses two distinct diverging length scales: one associated with the $SO(2)$ SW and the other associated with the Z_2 chirality. In that sense, the $SO(2)$ part and the Z_2 part are decoupled in this model. Reflecting the inequality $\nu'_s = 1/y'_s = 1 > \nu_\kappa = 1/y_\kappa = 0.5263 \dots$, however, the spin correlation is dominated by the chiral exponent ν_κ , not by the SW exponent $\nu'_s = 1$. *The inherent spin-chirality decoupling of the present model is then masked.*

These behaviors of the domain-wall energies and of the correlation lengths of the 1D $\pm J$ XY SG ladder are seemingly at odds with the behaviors of the corresponding 2D and 3D models suggested in Refs [10, 11]. In the 2D and 3D XY SG, Refs. ([10]) conjectured that $\Delta E_{P,AP}$ was governed by the $SO(2)$ spin exponent, while ΔE_c was governed by the Z_2 chiral exponent. This should be contrasted with the behavior of the present 1D model where $\Delta E_{P,AP}$ was governed by the Z_2 chiral exponent while ΔE_c was governed by the $SO(2)$ spin (SW) exponent. As argued in the previous section, however, this apparent difference is simply the consequence of the difference in the relative magnitude of the Z_2 and $SO(2)$ exponents between the two models. Indeed, in the 2D case, Ref.[10] estimated $y_\kappa \simeq 0.5$ and $y_s \simeq 1.0$ from the L -dependence of ΔE_c and $\Delta E_{P,AP}$, respectively, where one has $y_\kappa < y_s$ in contrast to the present 1D case. If the inequality between the two stiffness exponents y_κ and y'_s were opposite in the present 1D model, *i.e.*, $y_\kappa < y'_s$, essentially the same behavior as that in the 2D and 3D models, *i.e.*, $\Delta E_c \approx L^{-y'_s}$ and $\Delta E_{P,AP} \approx L^{-y_\kappa}$, would arise. Hence, the apparent large deviation from Ref.[10] is merely due to the difference in the relative magnitudes of the two stiffness (and correlation-length) exponents.

In this connection, a significant difference between the present 1D ladder model and the higher-dimensional models might be that, while the effective interaction between the charge variables m_i is short-ranged in 1D, that in higher dimensions is *long-ranged*. This assigns a non-trivial character to the charged excitation in the higher dimensional models. In 2D, this charged excitation could be viewed as a vortex. (In 3D, it is a vortex-line.) The im-

portant characteristic of such a vortex excitation is that it breaks the charge neutrality condition and interacts with each other via the long-ranged Coulombic interaction. In the present 1D ladder model, even though there certainly exists an excitation which apparently breaks the charge-neutrality condition, the associated interaction between them is always short-ranged, and cannot be regarded as a genuinely-charged vortex-like excitation.

Thus, in higher dimensions, excitations associated with the charge excitation are at least of two distinct types: The one is the vortex excitation which breaks the charge-neutrality, and the second one is the ordinary chiral excitation which preserve the charge-neutrality. In 2D, the former one is a point defect (vortex), while the latter is a line defect (domain-wall). Note that the former vortex-like excitation exists in both frustrated and unfrustrated XY spin models, often playing a vital role in the order-disorder process, while the latter chiral excitation is peculiar to the *frustrated* XY spin models. We expect that, in higher dimensions, this genuinely-charged vortex excitation might give rise to the another diverging length scale which predominantly disorder the spin (not the chiral) order. A possible conjecture would be that the stiffness exponent associated with the vortex excitation y_v takes a value smaller than the SW stiffness exponent or the chiral stiffness exponent, and is more effective in disordering the spin. If this is really the case, the spin correlation length and the domain-wall energy $\Delta E_{P,AP}$ would be governed by the non-chiral exponent y_v associated with the genuinely-charged excitation. In the 2D XY SG with the $\pm J$ interaction, the numerical estimate of Refs.[10] suggested $y_v \simeq 1$, which appears to be larger than $y_\kappa \simeq 0.5$.

We note that, even in 1D, the long-ranged interaction between the charge variables could arise in some special cases, *e.g.*, in the tube lattice investigated by Hill *et al* [22]. In the tube lattice, however, the application of neither the P, AP nor the R BCs is capable of generating the genuinely-charged vortex excitation, *i.e.*, the excitation in the q^+ variable in the notation of Ref.[22]. In fact, the application of either the P, AP and R BCs generates only the charge-neutral chiral excitation, the excitation in the q^- variable in the notation of Ref.[22], which interacts only via the short-ranged interaction. As such, the role of the genuinely-charged vortex excitation still remains to be seen in the 1D tube model. In order to elucidate the nature of the spin and the chirality orderings of the frustrated XY spin systems, it would be important to further clarify the role of the vortex-like genuinely-charged excitation, not only in the 1D tube model but also in the higher-dimensional models.

In the present paper, we concentrated on the XY SG ladder with the $\pm J$ interaction. The corresponding model with the Gaussian interaction was also studied in the literature, *e.g.*, in Ref.[23]. Our numerical study suggested that these two models, *i.e.*, the 1D XY SG ladder

with either the $\pm J$ or the Gaussian interaction exhibit quite different behaviors. The properties of the 1D XY SG ladder with the Gaussian interaction will be reported elsewhere [24].

APPENDIX: EFFECTIVE CHARGE HAMILTONIAN

In this appendix, we briefly summarize the derivation of the effective charge Hamiltonian corresponding to the original XY spin-glass model described by the spin Hamiltonian Eq. (1). We note that the Villain's Hamiltonian, which contains the two-body interaction between the charges only, is not exact even in the $T \rightarrow 0$ limit, contrary to a common belief. In the following, we give explicit forms of the correction terms to the Villain's approximation, which includes certain 4, 6,...body effective interactions between the charges. Details will be reported elsewhere within a more general context [26].

As usual, the starting point is the identity

$$e^{\beta \cos \theta} = \sum_{p=-\infty}^{\infty} e^{ip\theta} I_p(\beta), \quad (21)$$

where $\beta = 1/T$ is the inverse temperature and $I_p(\beta)$ is a modified Bessel function. Now we use a useful formula for the asymptotic behaviour in the limit $\beta \rightarrow \infty$,

$$\log \left(I_p(\beta) / \frac{e^\beta}{\sqrt{2\pi\beta}} \right) = \sum_{m=1}^{\infty} \frac{c_m}{m!} T^{2m-1} (1 + O(T)) \mu^m. \quad (22)$$

where $\mu = 4p^2$. Here terms which vanish in the $T \rightarrow 0$ are represented as $O(T)$. The first few coefficients reads as $c_1 = -1/8$, $c_2 = 1/192$, $c_3 = -3/2560$, $c_4 = 15/28672$, $c_5 = -35/98304$, $c_6 = 945/2883584, \dots$. Note that the usual Villain's approximation amounts to assume that $c_1 = -1/8$ and $c_m = 0$ for $m > 1$.

Following the standard steps of mapping of the original spin model to the charge model on the dual lattice [25], one finds that the effective charge Hamiltonian in the $T \rightarrow 0$ limit can be written as,

$$\mathcal{H}_{\text{charge}} = \mathcal{H}_{2\text{-body}} + \mathcal{H}_{4\text{-body}} + \mathcal{H}_{6\text{-body}} \dots \quad (23)$$

The terms on the r.h.s are due to the terms of $m = 1, 2, 3, \dots$ in Eqs. (22). The first term is nothing but the usual Villain's Hamiltonian which describes the two-body charge interactions,

$$\mathcal{H}^{2\text{-body}} = \sum_{i,j} U_{i,j} m_i m_j + \frac{2\pi^2}{L} (m_{\text{ex1}}^2 + m_{\text{ex2}}^2), \quad (24)$$

where $U_{i,j}$ is given by Eq. (5). The second term on the r.h.s describes global spin-wave excitations induced

by the two external charge variables m_{ex1} and m_{ex2} noticed in [21]. In the case of periodic (P) and antiperiodic (AP) boundary conditions (BC), all charge variables are subjected to the global neutrality condition $\sum_i m_i + m_{\text{ex1}} + m_{\text{ex2}} = 0$ due to the presence of a massless mode [21]. In the notation of §2, the external charges reads as $m_{\text{ex1}} = n - \frac{P}{2}$ for P BC and $m_{\text{ex1}} = n - \frac{P-1}{2}$ for AP BC while $m_{\text{ex2}} = \sum_i m_i - m_{\text{ex1}}$. One finds that the same global neutrality condition applies also for the higher-body terms given below for the cases of P and AP BCs. In the case of reflecting (R) boundary condition, on the other hand, one finds $m_{\text{ex1}} = m_{\text{ex2}} = 0$ in the dual mapping and also finds that the massless mode and thus the global neutrality condition is absent.

The explicit form of the higher-body terms becomes increasingly complicated. The 4-body Hamiltonian reads as,

$$\mathcal{H}^{4\text{-body}} = -\frac{4^2 c_2}{2!} \sum_i [D_i^4 + (D_{\text{ex1}})_i^4 + (D_{\text{ex2}})_i^4], \quad (25)$$

with

$$D_i \equiv \sum_j \left(\frac{U_{i+1,j}}{\pi} - \frac{U_{ij}}{\pi} \right) m_j, \quad (26)$$

$$(D_{\text{ex1}})_i \equiv -\frac{2\pi}{L} m_{\text{ex1}} + \sum_j \frac{U_{ij}}{\pi} m_j, \quad (27)$$

and

$$(D_{\text{ex2}})_i \equiv -\frac{2\pi}{L} m_{\text{ex2}} + \sum_j \frac{U_{ij}}{\pi} m_j. \quad (28)$$

The 6-body Hamiltonian reads as

$$\begin{aligned} \mathcal{H}^{6\text{-body}} = & -\frac{4^3 c_3}{3!} \sum_i [D_i^6 + (D_{\text{ex1}})_i^6 + (D_{\text{ex2}})_i^6] \\ & + \frac{1}{2} \left(\frac{2 \cdot 4^2 c_2}{1!} \right)^2 \left\{ \sum_{i,j} A_{ij} D_i^3 D_j^3 \right. \\ & - \sum_{i,j} (A_{ij} + B_{ij}) D_i^3 ((D_{\text{ex1}})_i^3 + (D_{\text{ex2}})_i^3) \\ & + \sum_{i,j} C_{ij} ((D_{\text{ex1}})_i^3 - (D_{\text{ex2}})_i^3) ((D_{\text{ex1}})_j^3 - (D_{\text{ex2}})_j^3) \\ & \left. + \frac{1}{L} \left[\left(\sum_i (D_{\text{ex1}})_i^3 \right)^2 + \left(\sum_i (D_{\text{ex2}})_i^3 \right)^2 \right] \right\}. \quad (29) \end{aligned}$$

where

$$A_{ij} = \frac{1}{L} \sum_k \frac{\cos(k(i-j))(1 - \cos(k))}{2 - \cos k}. \quad (30)$$

$$B_{ij} = \frac{1}{L} \sum_k \frac{\sin(k(i-j)) \sin(k)}{2 - \cos k}. \quad (31)$$

$$C_{ij} = \frac{1}{L} \sum_k \frac{\cos(k(i-j))}{4 - 2 \cos k}. \quad (32)$$

For a simple demonstration, let us consider a special 2-leg ladder sample in which all plaquettes are unfrustrated. In this particular sample, one knows that a spin-wave is induced under the AP boundary condition so that

$$\Delta E_{PAP} = -2L \left[\cos\left(\frac{\pi}{L}\right) - 1 \right] = \frac{\pi^2}{L} - \frac{1}{2!} \frac{\pi^4}{L^3} + \frac{1}{6!} \frac{\pi^6}{L^5} + \dots \quad (33)$$

exactly. One can check that the first three terms in the last equation can be obtained by the energies associated with the 2-body (Villain's approximation), the 4-body and the 6-body interactions, respectively.

-
- [1] J.R. Banavar and M. Cieplak, Phys. Rev. Letters **48**, 832 (1982).
- [2] W.L. McMillan, Phys. Rev. B **29** 4026 (1984).
- [3] A.J. Bray and M.A. Moore, J. Phys. C **17**, L463 (1984).
- [4] A.C. Carter, A.J. Bray and M.A. Moore, Phys. Rev. Letters **88**, 077201 (2002).
- [5] N. Kawashima and T. Aoki, J. Phys. Soc. Jpn. **69**, Suppl.A, 169 (2000); N. Kawashima, J. Phys. Soc. Jpn. **69**, 987 (2000)
- [6] See, for example, H. Kawamura, in *Quantum Properties of Low-Dimensional Antiferromagnets*, ed. Y. Ajiro and J.-P. Boucher (Kyushu University Press) p. 124 (cond-mat/0202109), and references cited therein.
- [7] J.M. Kosterlitz and N. Akino, Phys. Rev. Lett. **82** 4094 (1999).
- [8] E. Granato, J. Magn. Magn. Mater. **226**, 364 (2001); Phys. Rev. B **69**, 144203 (2004); *ibid.*, 012503 (2004).
- [9] L.W. Lee and A.P. Young, Phys. Rev. Letters **90**, 227203 (2003).
- [10] H. Kawamura and M. Tanemura, J. Phys. Soc. Jpn. **60** (1991) 608.
- [11] H. Kawamura, Phys. Rev. **B** 51 (1995)12398.
- [12] H. Kawamura and M.S. Li, Phys. Rev. Lett. **87**, 187204 (2001).
- [13] T. Horiguchi and T. Morita, J. Phys. Soc. Jpn. **59**, 888 (1990).
- [14] H. Kawamura and M. Tanemura, Phys. Rev. **B** 36 (1987) 7177.
- [15] G.G. Batrouni and E. Dagotto, Phys. Rev. **B** 37, R9875 (1988).
- [16] P. Ray and M. A. Moore, Phys. Rev. **B** 45, 5361 (1992).
- [17] H.S. Bokil and A.P. Young, J. Phys. **A29**, L89 (1996).
- [18] C. Wengel and A.P. Young, Phys. Rev. **B56**, 5918 (1997).
- [19] E. Granato, Phys. Rev. **B58**, 11161 (1998); **B61**, 391 (2000).
- [20] J. Maucourt and D. R. Grempel, Phys. Rev. Lett. **80** (1998) 770.
- [21] M. Ney-Nifle, H.J. Hilhorst and M.A. Moore, Phys. Rev. **B48** (1993) 10254.
- [22] M.J. Thill, M. Ney-Nifle and H.J. Hilhorst, J. Phys. A **28** (1995) 4285.
- [23] B.M. Morris, S.G. Colborne, M.A. Moore, A.J. Bray and J. Canisius, J. Phys. **C19**, 1157 (1986).
- [24] T. Uda and H. Kawamura, unpublished.
- [25] J. V. José, L. P. Kadanoff, S. Kirkpatrick and D. R. Nelson, Phys. Rev. B **16** 1217 (1977).
- [26] H. Yoshino and H. Kawamura, unpublished.